Image thresholding framework based on 2D fractional integration and Legendre moments'

A. Nakib, Y. Schulze, E. Petit

Published in IET Image Processing
Received on 11th October 2010
Revised on 28th November 2011
doi: 10.1049/iet-ipr.2010.0471

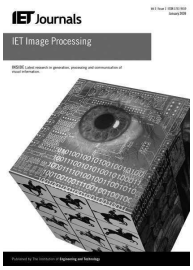

ISSN 1751-9659

Image thresholding framework based on two-dimensional digital fractional integration and Legendre moments'

A. Nakib Y. Schulze E. Petit

Laboratoire Images, Signaux et Systèmes Intelligents (LISSI, E. A. 3956), Université Paris EST-Créteil, 61 avenue du Général De Gaulle 94010, Créteil, France
E-mail: nakib@u-pec.fr

Abstract: In this study, the authors present a new image segmentation algorithm based on two-dimensional digital fractional integration (2D-DFI) that was inspired from the properties of the fractional integration function. Although obtaining a good segmentation result corresponds to finding the optimal 2D-DFI order, the authors propose a new alternative based on Legendre moments. This framework, called two dimensional digital fractional integration and Legendre moments' (2D-DFILM), allows one to include contextual information such as the global object shape and exploits the properties of the 2D fractional integration. The efficiency of 2D-DFILM is shown by the comparison to other six competing methods recently published and it was tested on real-world problem.

1 Introduction

Image segmentation methods allow one to extract an object from a background using some image features: grey level, colour, texture and position. It is the important step in an image processing system. Among the existing techniques, thresholding is one of the most popular approaches because of its simplicity, and multilevel thresholding plays an important role in segmenting an image into multiple meaningful regions and extracting their key features.

Many thresholding approaches have been developed over the past years [1–7]. For example, Bazi *et al.* [1] presented a parametric thresholding method. It finds the threshold through parameter estimation under the assumption that the object and background follow a generalised Gaussian distribution. Otsu's method [8] chooses the thresholds by maximising the ratio of between-class variance to the total variance. Kittler and Illingworth [3] determined the threshold by minimising the misclassification error (ME) probability. The method of Pun [5] achieves the threshold by maximising the a posteriori entropy of the object and background portions. Kapur *et al.* [9] found some flaws in Pun's derivations and presented a revised version. Wang *et al.* [7] determined the threshold by optimising a criterion function deduced by image histogram and the Parzen window technique.

Despite the multitude of image segmentation methods proposed in the last three decades [10], the quest for more effective methods continue. This is in part because of the necessity to handle as broad a category of images as possible and other part to meet the real-time demands in practical applications such as biomedical imagery.

The formalism of fractional order derivatives dates back to correspondence between Leibniz and L'Hospital in 1695 (see [11]). A significant advantage of fractional differentiation (derivative/integral) operators is that they can be applied to functions that are not differentiable in the classical sense. Unlike the integer order differentiation, the fractional order differentiation at point x is not defined by an arbitrary small neighbourhood of x. In other words, the fractional differentiation is not a local property of a function. There exist several well-known approaches to unification of differentiation operators (integral and derivative), and their extension to non-integer orders [12]. Recently, fractional differentiation has found applications in various areas: in control theory, it is used to determinate a robust command control [13]; it is also used to solve the inverse heat conduction problem [14]; other applications are reported for instance in neuronal modelling [15], in image processing [16–18] and in biomedical signal processing [19].

In this paper, we propose a method that addresses the major drawbacks of classical thresholding methods: the lack of the homogeneity of the solution, and the disregard of the spatial distribution of pixels. Indeed, the proposed method makes use of properties of the two-dimensional digital fractional integration (2D-DFI). In this work, we show that using 2D-DFI with an optimal order can provide better results than previous approaches based on fractional derivation. Then, to find the optimal the 2D-DFI order, we propose to use the moments of Legendre. The whole proposed method is called, two dimensional digital fractional integration and Legendre moments' (2D-DFILM).

The paper is organised as follows. In Section 2, the 2D-DFI function is presented. In Section 3, we describe and analyse

the proposed thresholding method based on 2D-DFI with an arbitrary order. The optimisation of the 2D-DFI order using Legendre moments' is described in Section 4. The performance of the proposed algorithm is discussed in Section 5. Finally, we conclude in the last section.

2 Two-dimensional digital fractional integration

In this section, we present the formalism of the 2D fractional integration. Then, some of the properties of the 2D-DFI that will be exploited are also presented and analysed.

The one-dimensional fractional integrals introduced by Grünwald–Letnikov for a real continuous function $f(t)$, is expressed as follows [20, 21]

$$f^{(\alpha)}(t) = \lim_{\substack{h\to 0 \\ kh=t-c}} \frac{1}{h^{-p}} \sum_{j=0}^{k} \begin{bmatrix} \alpha \\ j \end{bmatrix} f(t-jh) \tag{1}$$

where $\alpha \in \Re^{-*}$ is the fractional integral order, $\rho \in \Re^{+*}$ and $\begin{bmatrix} \alpha \\ j \end{bmatrix} = (\alpha \cdot (\alpha+1) \cdots (\alpha+j-1)/j!)$, and $j!$ means the factorial of j. c and t are real constants and correspond to the upper and the lower limits of the differentiation.

For fixed k (the upper limit of the summation), the fractional integral function, $f^{(\alpha)}(t)$, goes to 0, when $h \to 0$. To constrain $f^{(\alpha)}(t)$ to tend to non-zero limit, we have to assume that $k \to \infty$ when $h \to 0$. Then, we denote the limit of $f^{(\alpha)}(t)$ by

$$\lim_{\substack{h\to 0 \\ kh=t-c}} f^{(\alpha)}(t) = D^{\alpha}_{c,t} f(t) \tag{2}$$

In this paper, we consider the approximation of the discrete fractional integration given by

$$\tilde{D}^{\alpha} f(t) = \sum_{j=0}^{k} \begin{bmatrix} \alpha \\ j \end{bmatrix} f(t-j) \tag{3}$$

For simplicity, it is convenient to assume that $c = 0$, and the sampling step $h = 1$ and the number of nodes k is related by $t = kh$. Definition (3) shows that the fractional integral of a function at t takes into account the past of the function f.

As an image can be considered as a 2D real bounded function $f(x, y)$, the approximation of the fractional integrated image is then given by

$$\tilde{D}^{\alpha} f(x,y) = \sum_{k=-\lfloor M/2 \rfloor}^{\lfloor M/2 \rfloor} \sum_{l=-\lfloor N/2 \rfloor}^{\lfloor N/2 \rfloor} \begin{bmatrix} \alpha \\ k \end{bmatrix} \begin{bmatrix} \alpha \\ l \end{bmatrix} f(x-k, y-l) \tag{4}$$

where M and N represent the number of past elements of f considered to calculate the fractionally integrated image. $M \times N$ represents the size of the 'mask', and $\lfloor x \rfloor$ denotes integer parts of x.

We define the values of the approximation of the fractionally integrated pixels by

$$g^{\alpha}(x,y) = \begin{cases} L & \text{if } \tilde{D}^{\alpha} f(x,y) \geq L \\ 0 & \text{if } \tilde{D}^{\alpha} f(x,y) \leq 0 \\ \tilde{D}^{\alpha} f(x,y) & \text{otherwise} \end{cases} \tag{5}$$

where L is the total number of grey levels.

2.1 Properties of the integrated image

In this section, we present a statistical interpretation of the application of 2D-DFI to a 2D-function or an image. We also propose to observe the average value of the integrated image.

2.1.1 Homogeneity: To illustrate the application of the 2D-DFI to an image, we consider the image of a plane in Fig. 1*a*. To analyse the transformation achieved on the image features, the entropy of the integrated image for a given 2D-DFI order (α) is calculated.

The homogeneity of the image is increased by the application of 2D-DFI to the original image. To measure this homogeneity we used the entropy measure of the image. It is known that the entropy decreases with the increasing of the image homogeneity (non-uniformity of its histogram). In Fig. 2, we can see this variation of image homogeneity (image of Fig. 1*a*) for different values of 2D-DFI order. It can be noted that entropy decreases in a 'linear' way with the decrease of 2D-DFI order from 0 to -1; that behaviour corresponds also to an increase in a linear way of the image homogeneity.

2.1.2 Average value: From expression (4), the function $g^{\alpha}(x, y)$ can be interpreted as the output image of a discrete filter, where $f(x, y)$ is the input image. The transfer function, with discrete Fourier variables u and v which correspond to the real variables x and y is

$$H^{\alpha}(u,v) = \frac{G^{\alpha}(u,v)}{F(u,v)} = \frac{1}{MNh^{2\alpha}} \sum_{k=0}^{M-1} \sum_{l=0}^{N-1} p(k,l) \exp^{-h\alpha((u/N)k+(v/M)l))} \tag{6}$$

From (6), we can easily show (by using the properties of the 2D Fourier transform) that the average value of the output image, or the integrated 2D function, is defined by

$$\mu_g^{\alpha} = \mu_f \times H(0,0) = \mu_f \times \frac{1}{MNh^{2\alpha}} \sum_{k=0}^{M} \sum_{l=0}^{N} p(k,l) \tag{7}$$

where μ_f and μ_g^a are the average values of the functions f and g for a given α, respectively, H is the 2D Fourier transform of $h(x, y)$. This assertion can also be interpreted from the amplitude frequency responses in Fig. 3. From this analysis we can explain the pixels' grey-level decrease over all the images.

3 Image thresholding with an arbitrary 2D-DFI order

In this section we present the proposed segmentation algorithm with 2D-DFI with an arbitrary order (α). Before presenting the segmentation algorithm, we first analyse the 2D-DFI. Then, we show that the segmentation problem can be solved using 2D-DFI. We end this section, with the presentation of 2D-DFI algorithm.

In the previous works [18], the authors differentiate fractionally the histogram of the original image in order to separate the different classes. In [17], the authors differentiate fractionally (derivate) the image and segment it using its resulting histogram. Here, we fractionally integrate

doi: 10.1049/iet-ipr.2010.0471

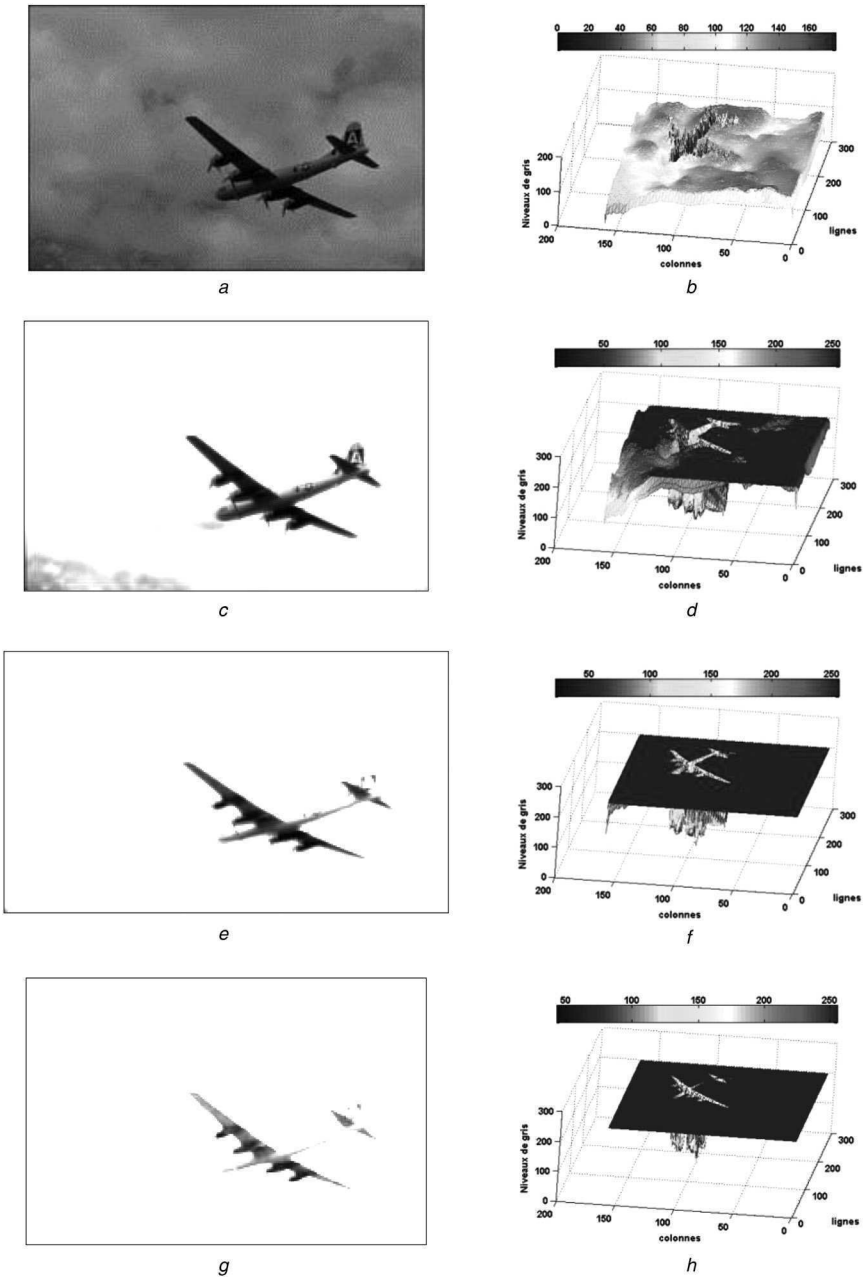

Fig. 1 *Modification of the dynamic of the image using 2D-DFI with different orders*

a Original image
b Original dynamic of the image
c Integrated image with $\alpha = -0.3$
d Variation of the dynamic of the integrated image for $\alpha = -0.3$
e Integrated image with $\alpha = -0.5$
f Variation of the dynamic of the integrated image for $\alpha = -0.5$
g Integrated image with $\alpha = -0.9$
h Variation of the dynamic of the integrated image for $\alpha = -0.9$

the original image and segment it without looking at its histogram.

In [17] the properties of 2D-DF differentiation mask are analysed. Indeed, in the one-dimensional case, authors in [19] showed the correlation between the fractional integration filters and band pass filters. The geometric properties of the fractional are the opposite of those of the fractional differentiation. In other words, the homogeneity of the image increases in an exponential way when the 2D-DFI order goes from 0 to -1. In Figs. 3*a*–*d*, we present the frequency responses of the fractional integral masks for different 2D-DFI order (α): -0.1, -0.2, -0.4 and -0.6, respectively. As one can remark, when the 2D-DFI order increases, the contrast between the object and the background is increased, and the noise reduction also increases. This figure demonstrates the noise reduction achieved by using these masks, this remark was also claimed in [16, 17]. It explains also how the removal of the background is achieved in Fig. 1, where only the foreground appears. Indeed, these masks operate as a kind of low-pass or band pass filters.

The algorithm consists of three steps: calculating the mask with a given 2D-DFI order, filtering the input image and thresholding the image. It is summarised in Algorithm 1.

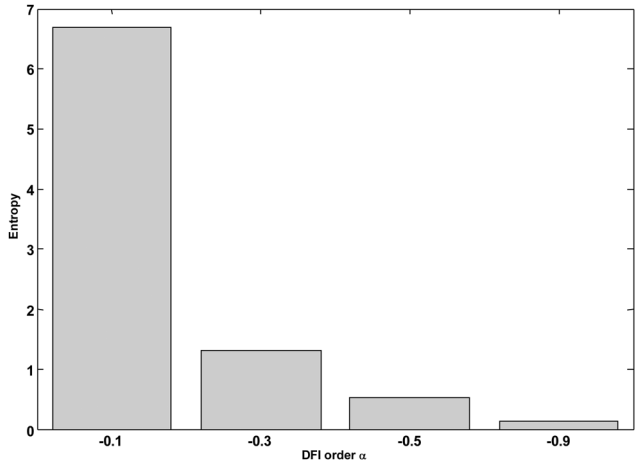

Fig. 2 *Variation of the entropy of the original image in Fig. 1a for different 2D-DFI order*

Fig. 4 shows an example of the thresholding using different DFI order. Fig. 4*a* is a moon image from Matlab Mathworks database, Fig. 4*b* illustrates an optimal segmentation result with DFI order equal to -0.1 and Fig. 4*c* presents a segmentation result with -0.35.

Looking at the different results in Figs. 1 and 4, one can remark that the segmentation problem is transformed to another problem that consists of finding the optimal 2D-DFI order that allows to have a good image segmentation results.

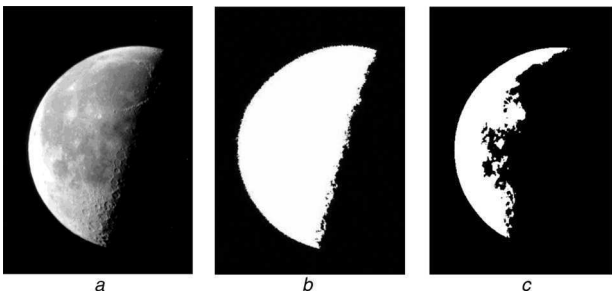

Fig. 4 *Illustration of thresholding algorithm*

a Original image
b Thresholded image with -0.1
c Thresholded image with -0.35
The segmentation threshold was fixed to *L*-2 for all images

Algorithm 1: Segmentation algorithm 2D-DFI.

1. **Calculate** the 2D-DFI mask for a given 2D-DFI order (α).
2. **Filter** the original image using the obtained mask using expression (4).
3. **Threshold the image** using expression (5).
4. **Print** the segmentation result.

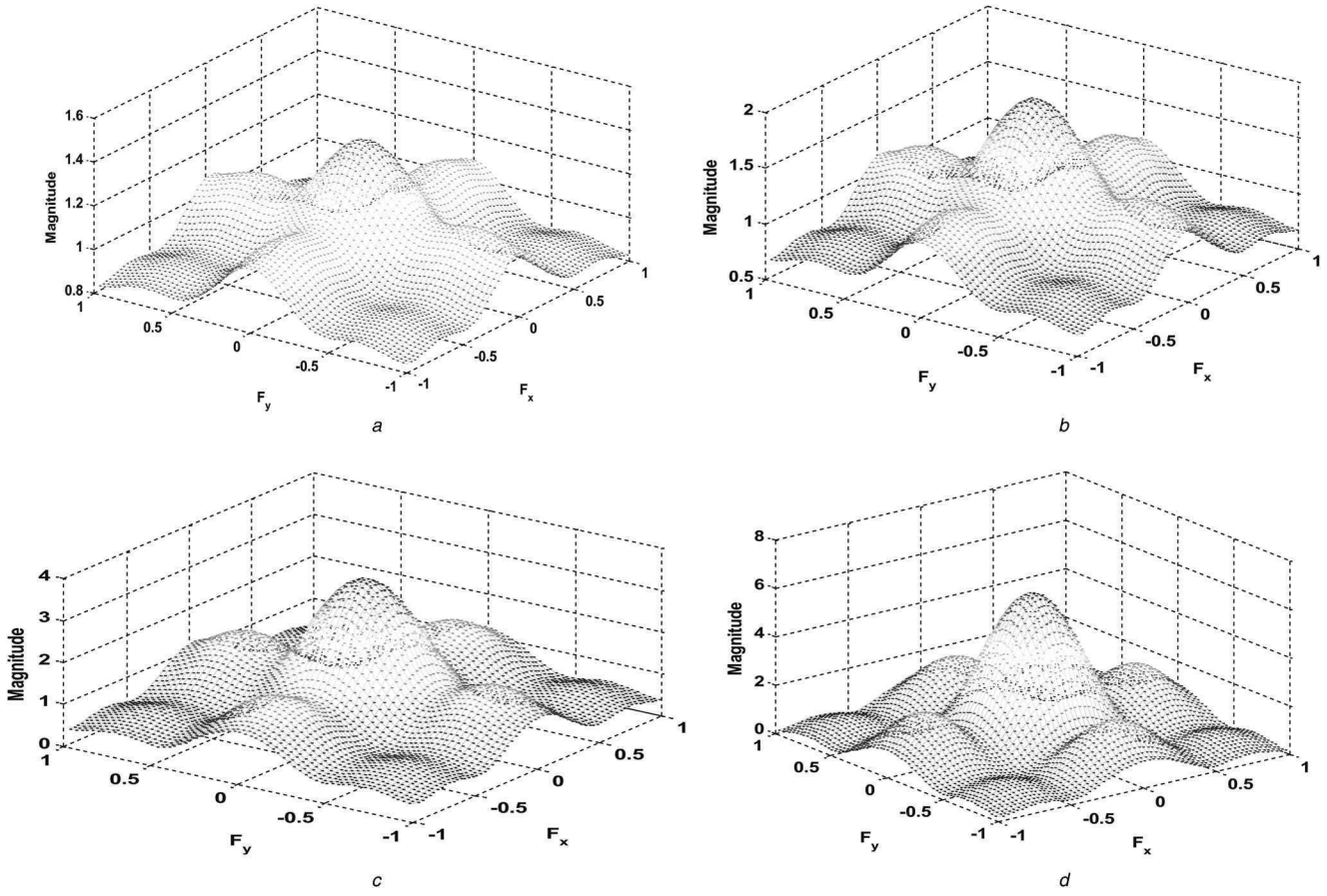

Fig. 3 *Frequency response of different 2D-DFI masks*

a $\alpha = -0.1$
b $\alpha = -0.2$
c $\alpha = -0.4$
d $\alpha = -0.6$

doi: 10.1049/iet-ipr.2010.0471

4 Optimisation of the 2D-DFI order

In this work, we propose to use the notion of prior shape based on the Legendre moments' to find the optimal 2D-DFI order. In the following sections, we present briefly the principles of calculation of the moments and from a prior shape.

4.1 Legendre moments'

We define contextual information as the global object shape. We propose to use Legendre moments' computed from the geometric centred and normalised moments as shape descriptor because they provide a parametric representation that can be made intrinsically invariant to affine transformations and from which a shape prior can be naturally defined in terms of distance or probability.

We consider that a shape can be represented by a function $f(x,y)$, where f is a binary function that associates 1 at all points inside the object and 0 outside of this object. In the following, we name Ω_{int} the set of pixels that defines the region inside the object (including its edges) and Ω_{ext} the set of pixels that belongs to the rest of the image (see Fig. 5).

In the literature, most of approaches [22–24] use a reference shapes. Usually, this reference consists of a binary image and gives general information about the shape to find.

The basic idea is to encode the geometry of the segmented object and that of the reference shape using a set of parameters that are gathered in shape descriptors. Then, the geometric constraint is defined as the distance between the two descriptors. In our case, we consider the descriptor of the reference image and that of the segmented image using 2D-DFI. These descriptors are defined by the projection of the characteristic function of the image $f(x, y)$ on an identified basis.

Our goal is to build a basis using the orthogonal Legendre polynomials calculated from the centred and normalised geometric moments. This method allows to have the property of scale and translation invariance that solves the problem of the alignment of the two shapes (reference and segmented one) and their sizes.

4.1.1 Geometric moments: The projection of the characteristic function on polynomial basis $\{x^p\ y^q\}$, where $p+q$ is the order of the moment, allows to define the set of the geometric moments $\{M_{p,q}, (p, q) \in \mathbb{N}^2\}$ by

$$M_{p,q} = \int\int_{\Omega} x^p y^q f(x)\,\mathrm{d}x\mathrm{d}y = \int\int_{\Omega_{\text{int}}} x^p y^q\,\mathrm{d}x\mathrm{d}y \tag{8}$$

The scale and translation invariance can be obtained by changing the basis, the new basis has the barycentre of the object $(\bar{x}, \bar{y})$ as origin. Then, we define the moments by

$$M_{C_{p,q}} = \int\int_{\Omega_{\text{int}}} (x-\bar{x})^p (y-\bar{y})^q\,\mathrm{d}x\mathrm{d}y \tag{9}$$

The scale invariance can be easily obtained by changing the variables [23, 24]. Then, the geometric moments (centred and normalised) are defined by

$$\eta_{p,q} = \frac{1}{|\Omega_{\text{int}}|^{(p+q+2)/2}} \int\int_{\Omega_{\text{int}}} (x-\bar{x})^p (y-\bar{y})^q\,\mathrm{d}x\mathrm{d}y \tag{10}$$

where $|\Omega_{\text{int}}|$ is the area of the object, and $(x, y) \in [-1, 1] \times [-1, 1]$ as in [24]. The coordinates (x, y) are defined by

$$\begin{cases} x_i = -1 + \left(i - \dfrac{1}{2}\right)\Delta x \\ y_j = -1 + \left(j - \dfrac{1}{2}\right)\Delta y \end{cases} \tag{11}$$

and

$$\begin{cases} \Delta x_i = \dfrac{2}{M} \\ \Delta y_j = \dfrac{2}{N} \end{cases} \tag{12}$$

$M \times N$ is the size of the image, $i = 1, 2, \ldots, M$ and $j = 1, 2, \ldots, N$.

The basis used for computing the geometric moments is not orthogonal. As some problems coming from the redundancy of the information appear, we use the Legendre polynomials basis.

However, other geometric moments can be used as: Zernik moments' and the angular radial transform used in MPEG-7 but geometric moments that are not invariant to rotation as Hu moments' cannot be used and require reformulation.

4.1.2 Normalised and centred moments of Legendre: The polynomials of Legendre are denoted by $P_n(x)$ and exist in the interval $[-1, 1]$. Generally, they are defined by

$$P_n(x) = \frac{1}{2^n n!} \times \frac{\mathrm{d}^n}{\mathrm{d}x^n}(x^2-1)^n \tag{13}$$

where n is the order of the polynomial. A recursive formulation of these polynomials is given in [24]. Using these polynomials we define the moments of Legendre with $\Omega \subset [-1, 1] \times [-1, 1]$

$$\lambda_{p,q} = \frac{(2p+1)(2q+1)}{4} \int\int_{\Omega_{\text{int}}} P_p(x) P_q(y)\,\mathrm{d}x\mathrm{d}y \tag{14}$$

In the following we denote $C_{p,q} = ((2p+1)(2q+1)/4)$.

The polynomials of Legendre can be also described by the following formula

$$P_n(x) = \sum_{i=0}^{n} a_{ni} x^i \tag{15}$$

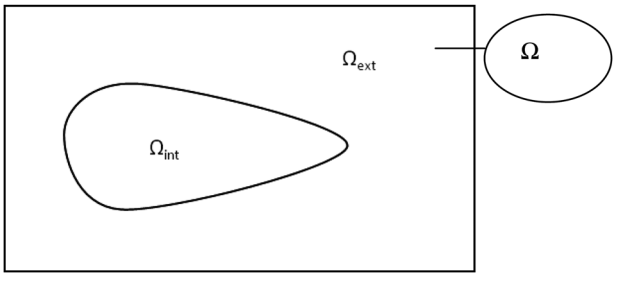

Fig. 5 *Illustration of the set Ω*

where the coefficients $a_{n,i}$ are defined by [25] (see (16))
The use of this formulation of the polynomial shows the relation between the geometric centred and normalised moments (8) and the centred and normalised Legendre moments' (16). Then, we obtain the centred and normalised Legendre moments:

$$\lambda_{p,q} = C_{p,q} \sum_{i=0}^{p} \sum_{j=0}^{q} a_{p,i} a_{q,j} \eta_{i,j} \tag{17}$$

4.1.3 Application of the geometrics shape constraints to the segmentation problem: In this paragraph, we introduce the notion of geometric shape constraints. We first define energy of shape prior

$$J_{\text{form}}(\Omega_{\text{int}}) = \int\int_{\Omega_{\text{int}}} \| \lambda(\Omega_{\text{int}}) - \lambda^{\text{ref}} \|^2 \tag{18}$$

where $\lambda(\Omega_{\text{int}})$ are the normalised and centred Legendre moments' for the segmented image and λ^{ref} for the reference image.

Our goal is to compare the Legendre moments' of the reference and the segmented shapes. Indeed the 2D-DFI order is optimal when the difference is minimal, which means that we want to find the order which minimises J_{form}.

We can finally describe the problem as following

$$\alpha^* \text{ such as } J^{\alpha^*}_{\text{form}}(\Omega_{\text{int}}) = \underset{\alpha \in [-1,0]}{\text{Min}} J^{\alpha}_{\text{form}}(\Omega_{\text{int}}) \tag{19}$$

where α^* is the 2D-DFI optimal order and $J^{\alpha}_{\text{form}}(\Omega_{\text{int}})$ the energy of shape prior for an image segmented with α.

4.2 Proposed algorithm

We propose an algorithm that consists of two main procedures: the application of 2D-DFI, then the LM, for finding the optimal order. The drawback of classical thresholding methods is that segmented objects are not homogenous (pixels of the object are not totally connected or consists of two regions). To avoid this problem, we use LM to test every connected region and save only that minimises the criterion J_{form} defined in (18). After testing all values of the 2D-DFI order, the segmented region that has the minimal value corresponds to the segmentation result.

We can summarise the proposed algorithm on three main steps. The first consists of the calculation of the geometric moments of the reference image (Fig. 6).

5 Results and discussions

In this section, we present the obtained segmentation results using the proposed method, called 2D-DFILM, we performed a comparison to six other methods: Otsu method [8], Kapur *et al.* method [9], thersholding using digital fractional differentiation (TDFD) method [18], one method based on valley emphasis (VE) method [26], expectation maximization (EM)-based algorithm method (EM) [1] and Sahoo and Arora [27] method based on 2D Tsallis entropy

1. Calculation of the Legendre moments' of the reference image
2. For α from -1 to 0 (step size 0.05):
   a. Application of the DFI with the α order
   b. Thresholding of the Integrated image
   c. *For each connected component*
      i. Calculation of the Legendre moments' for the current component (all the other components are eliminated)
      ii. Calculation of J^{α}_{form}
   d. Search of the minimal J^{α}_{form} and the α^* corresponding
3. Display of the image segmented by DFI with the order α^*

Fig. 6 *2D-DFILM algorithm*

(TE), using synthetic images. Then, we present results on other testing images from free Berkely University images database [28]. This section ends with the segmentation results on real-world application.

The proposed method was coded in Matlab version 7 and run on the Intel Xeon 6 (X5650) processor at 2.66 GHz, under Sentos (Linux) Operating system.

5.1 Performance analysis based on synthetic images

In this experience, we used a synthetic image with different degrees of noise (Fig. 7). The images in Figs. 7*a–c* correspond to the image in Fig. 7(1) noised by different degrees of a multiplicative noise. Figs. 7*d–f* correspond to the image in Figs. 8*a–c* noised by an additive white Gaussian noise, respectively.

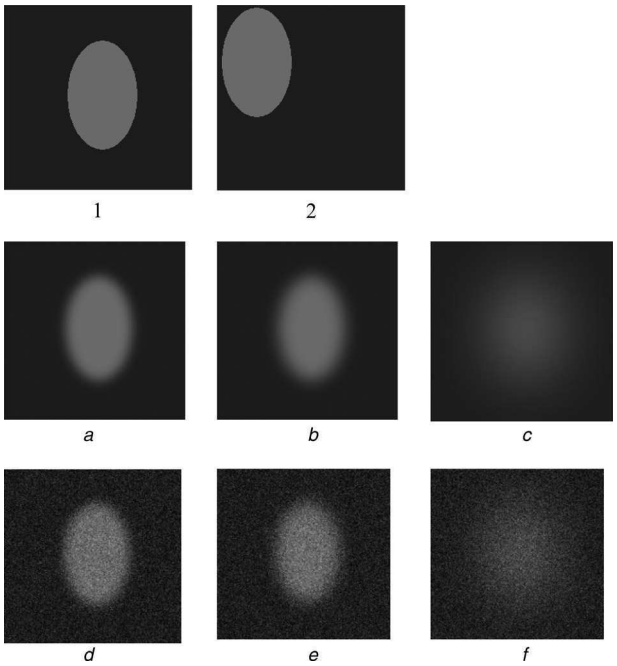

Fig. 7 *Original and noised synthetic images*
1 Original image
2 Reference image
a–f Noised synthetic images

$$a_{n,i} = \begin{cases} (-1)^{(n-i)/2} \dfrac{1}{2^n} \times \dfrac{(n+i)!}{((n-i)/2)!((n+i)/2)!i!}, & \text{if} \quad (n-i) \text{ even} \\ 0, & \text{otherwise} \end{cases} \tag{16}$$

doi: 10.1049/iet-ipr.2010.0471

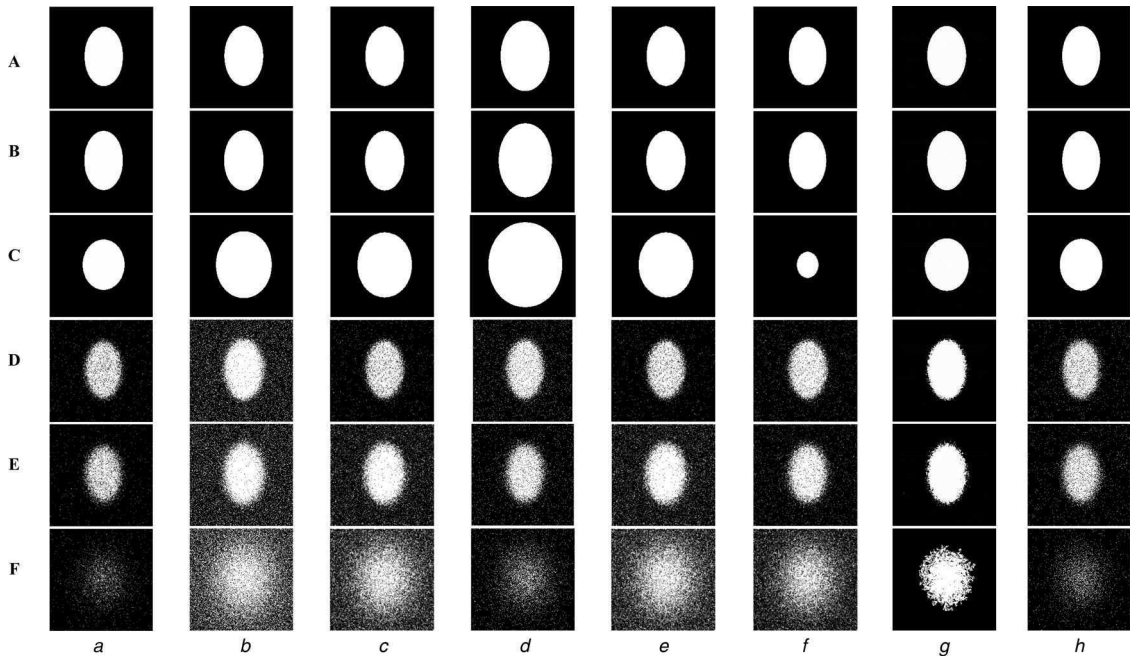

Fig. 8 *Performance analysis on synthetic images*

a Segmented images by TDFD
b Segmented images by Otsu
c Segmented images by Kapur_M
d Segmented images by EM method
e Segmented images by VE
f Segmented images by TE
g Segmented images by 2D-DFILM
h Segmented images by 2D-DFD

In order to compare the performance of the proposed method the six other methods, mentioned above, we used a synthetic image with different degrees of noise (Fig. 7). To measure the performance of these methods, we used the ME criterion [10]. ME is defined in terms of correlation of the images with human observation. It corresponds to the ratio of foreground pixels incorrectly assigned to the background, and vice versa. Then, ME is defined by

$$\mathrm{ME}(\%) = \left(1 - \frac{|B_{\mathrm{O}} \cap B_{\mathrm{T}}| + |F_{\mathrm{O}} \cap F_{\mathrm{T}}|}{|B_{\mathrm{O}}| + |F_{\mathrm{O}}|}\right) \times 100 \qquad (20)$$

where background and foreground are denoted by B_{O} and F_{O} for the original image, and by B_{T} and F_{T} for the thresholded image, respectively. In the best case of ideal thresholding, ME is equal to 0% and, in the worst case, ME value is 100%.

The comparison of the results provided by our method and the six other methods, based on the segmentation of synthetic images, is presented in Fig. 8. Table 1 presents a quantitative study of these results. As it can be seen, the proposed method provides (Fig. 9*a*) better results than the other methods, only TDFD method provides a similar performance (Table 1, image A), in this a low multiplicative noise was applied to the original image [Fig. 7(1)]. As it can be seen, with the increase of the noise, the proposed algorithm outperforms all other competing methods. In order to show the efficiency of the use of LM (in our experiments we used LM with the order 15), the reference image is presented in Fig. 7(2), where the object is not in the same place as in Fig. 7(1).

5.2 Image thresholding examples

In this subsection we present some segmentation results to illustrate the performance of the proposed method, and we end this subsection by showing its limitations.

In Fig. 8 with the original plane image is given in Fig. 1*a*. In this example, the goal is to extract the plane from the

Table 1 Performance evaluation of the proposed method compared to competing methods

Image	Segmentation methods										
	Otsu [8]	Kapur *et al.* [9]	TDFD [18]		EM [1]	VE [26]	TE [27]	2D-DFILM		2D-DFD [17]	
	ME, %	ME, %	α	ME, %	ME, %	ME, %	ME, %	α	ME, %	α	ME, %
A	0.45	5.61	0.60	0.17	8.68	0.34	0.64	−0.35	**0.20**	0.13	**0.17**
B	0.82	4.50	0.10	0.39	12.50	0.63	1.12	−0.35	**0.27**	0.13	0.40
C	12.21	4.97	0.40	3.30	28.87	11.59	12.90	−0.4	**2.87**	0.09	3.39
D	11.80	5.77	−0.83	5.71	5.74	5.90	5.90	**−0.34**	**1.06**	0.47	5.61
E	14.93	6.74	−0.82	6.51	6.60	13.22	6.58	**−0.35**	**1.51**	0.45	6.82
F	36.80	17.66	−0.58	15.78	15.86	35.56	29.98	**−0.4**	**6.43**	0.26	15.89

background. The used reference image is presented in Fig. 9*a*, one can see that the reference image is a simple picture of a plane. The segmentation result using 2D-DFILM is presented in Fig. 9*b*, where one can see the efficiency of the proposed method. In order to evaluate the quality of the segmentation result with different prior shapes that we present in Figs. 9*a*, *c*, *e*, *g*, *i* and *k*, and their corresponding segmentation results are presented in Figs. 9*b*, *d*, *f*, *h*, *j* and *l*, respectively. One can remark that in most of the cases obtained results are very good. However, in the case of the prior shape of Fig. 9*g* the proposed fails, this result can be explained by the geometry of the prior shape. As we can see, this shape presents only the profile view of a plane, consequently, the 2D-FILM converges

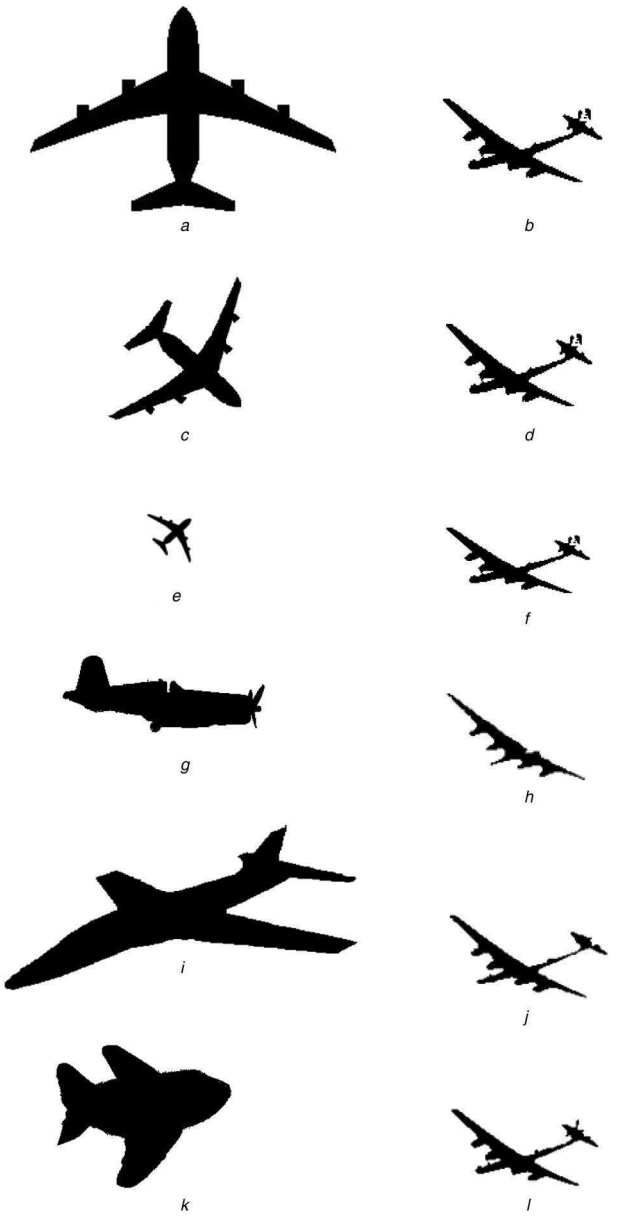

Fig. 9 *Illustration of the performance of DFLIM method with LM order equal to 5 via the Segmentation of the original image presented in Fig. 2a with different reference image*

b 2D-DFILM segmentation result with $\alpha = -0.5$ using reference image in *a*
d 2D-DFILM segmentation result with $\alpha = -0.5$ using reference image in *b*
f 2D-DFILM segmentation result with $\alpha = -0.5$ using reference image in *e*
h 2D-DFILM segmentation result with $\alpha = -0.75$ using reference image in *g*
j 2D-DFILM segmentation result with $\alpha = -0.55$ using reference image in *i*
l 2D-DFILM segmentation result with $\alpha = -0.5$ using reference image in *k*

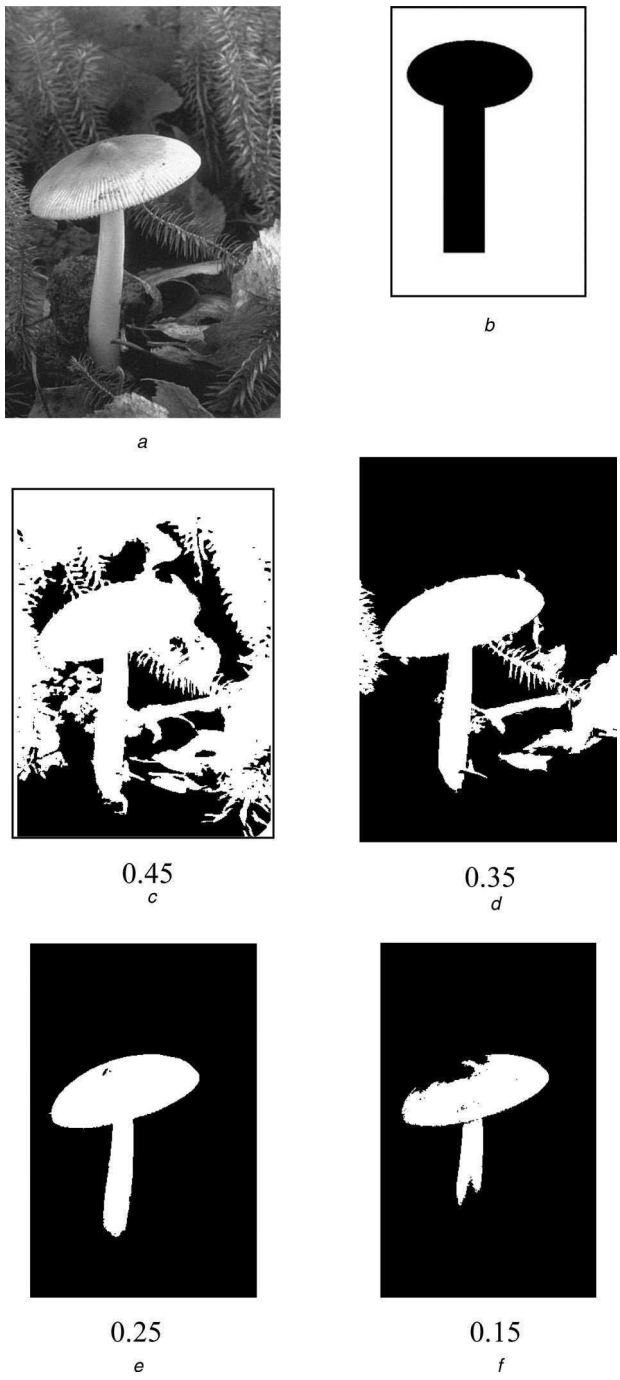

Fig. 10 *Illustration of the performance of DFILM method*

a Original image
b Reference image
c Segmentation result with $\alpha = -0.45$
d Segmentation result with $\alpha = -0.35$
e Segmentation result with $\alpha = -0.25$
f Segmentation result with $\alpha = -0.15$
For all experiments LM order is 5. The optimal segmentation result selected by 2D-FILM is that presented in *e*

Table 2 2D-DFILM execution time analysis. In this example, we segmented the original image an image of Fig. 1*a*

LM order	LM time, s	2D-DFILM time, s
5	0.21	2.1
10	0.60	5.4
15	1.29	10.8
25	3.34	25.26
50	12.52	76.93

doi: 10.1049/iet-ipr.2010.0471

to a shape that looks like a profile, and the segmentation procedure fails.

A second example is presented in Fig. 10. In this case, the goal is to extract the mushroom from the background. The original image is in Fig. 10*a*, the reference image is in Fig. 10*b* that represents an approximate shape of a mushroom. The different segmentation results with different 2D-DFI order, -0.45, -0.35, -0.25 and -0.15 are presented in Figs. 10*c–f*, respectively. The optimal segmentation result [that minimises the J^{α}_{form} criterion (17)] is that presented in Fig. 10*e*. One can see that the mushroom is well extracted from the background. Then, the optimal value of the 2D-DFI order that allows this result is $\alpha = -0.25$, the order of the Legendre moments' is 5.

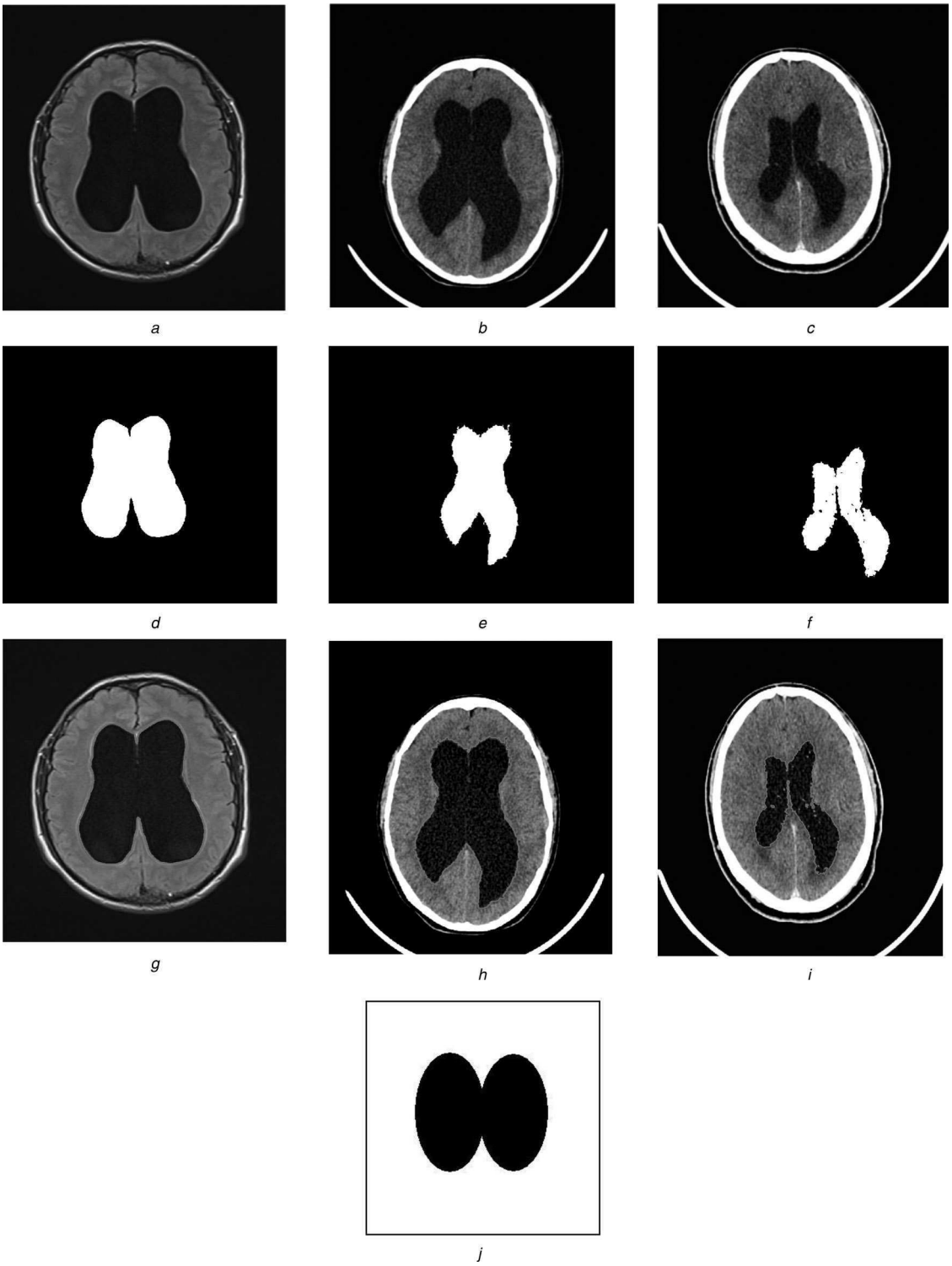

Fig. 11 *Segmentation of pathologic medical images*

a Original MRI image
b and *c* Original CT-scan images
d–f Segmentation results of images in *a–c* using 2D-DFILM ($\alpha_{\text{opt}} = -0.15$, -0.40 and -0.55, respectively)
g–i Superposition of the original image and the segmentation results
j Reference image

The limitations of the proposed method are mainly related to the use of Legendre moments'. Indeed, 2D-FILM computes Legendre moments as zero-order approximation, in comparison with the theoretical definition. This means that the computation of the moments is not accurate instead some approximation errors are generated. These errors affect not only the reconstruction performance of the corresponding moments but also their discriminative ability. Hosny [24] presented promising results, which calculate the exact previous moment values.

Another limitation was observed: in the case of strongly textured images, the contrast enhancement achieved by the 2D-DFI is not enough to allow different parts of an object to be extracted at the same time. Then, objects cannot be extracted even if we use high-order moments. For every 2D-DFI order, we will extract only a part of the object. So, in this case deformable-based methods are more suitable.

5.3 Computation complexity analysis

In this subsection, we present the computation complexity of the proposed

- The computational complexity of the 2D-DFI is given by: $O(S)$ for a given 2D-DFI order α, where S is the total number of pixels in the image and $O(.)$ is Landau's function.
- The Legendre moments' requires $O(q \times p^3 + p \times q^3)$ operations, where $p + q$ is the order of the moments.

Therefore the total computational complexity of the proposed method is $O(q \times p^3 + p \times q^3) + O(S)$ for a given 2D-DFI order α.

One can remark that the complexity of the 2D-DFI is lower than the other competing methods because it consists of applying the approximated fractional filter but the optimisation of the order increases its complexity.

It is clear that the proposed 2D-DFILM method is more complex than the other methods from the literature. However, the proposed can be parallelised easily and its execution can decrease drastically.

In Table 2, we present the different execution time, in this case our programme was not parallelised. The execution time does not vary a lot from an image to another because the complexity does not depend on the image size.

5.4 Real-world application

To illustrate the results of our segmentation algorithm on real-world medical images, examples of brain magnetic resonance images (MRI) and CT-scan images are presented in Fig. 11. In this example, the presented pathology is the hydrocephalus, also known as 'water on the brain' and is a medical condition in which there is an abnormal accumulation of cerebrospinal fluid in the ventricles, or cavities, of the brain. The goal is to evaluate the size of the ventricles in order to evaluate the pathology. The original MR images are presented in Figs. 11*a*–*c*, CT-scan images and their segmentations are presented in Figs. 11*d*–*f*, and the superposition of the segmentation result on the original image is in Figs. 11*g*–*i*, respectively. Then, the reference image is in Fig. 11*j*.

One can see that the segmentation results are good in most of the cases independently of the modality of the acquisition (MRI or CT-scan). The segmentation result of the image in Fig. 11*c*, that is a CT-scan image, present some halls inside the segmented region. This example shows the limitation of the proposed method. Indeed, the proposed method can fail in the case of strongly textured images. To solve this problem, one can perform a morphological closing to achieve a fully homogeneous segmentation result.

6 Conclusions

In this paper, a new segmentation method based on 2D-DFILM was presented. This method uses fractional differentiation with negative order that corresponds to a fractional integration. The different frequency characteristics of the filter were also presented. The proposed method allows segmenting any image with any 2D-DFI order. To find the best segmentation or the optimal 2D-DFI order, the Legendre moments' were used. The proposed method, need an approximate reference image for performing segmentation, it does not need a very detailed description of the shape that the user wants to extract. In the introduction, we presented the problem of thresholding methods: regions in the same class are not always connected. This problem was solved, by the use of LM to find the optimal connected component that is similar to the reference image. If the reference image is not available, the Legendre moments' cannot be used. In this case, one can use the 2D-DFI algorithm to segment an image but the optimal order has to be fixed.

We demonstrated, through some examples, that the proposed thresholding method outperforms the classical entropic thresholding method of Kapur *et al.* [9], Otsu's thresholding method [8] and other methods recently published [1, 18, 26, 27].

In work in progress, we hybrid the proposed method with level set based methods and graph cut methods. We also work on the relation between the wavelet transform and the fractional differentiation.

7 References

1 Bazi, Y., Bruzzone Melgani, F.: 'Image thresholding based on the EM algorithm and the generalized Gaussian distribution', *J. Pattern Recognit.*, 2007, **40**, pp. 619–634
2 Horng, M.: 'A multilevel image thresholding using the honey bee mating optimization', *Appl. Math. Comput.*, 2010, **215**, (9), pp. 3302–3310
3 Kittler, J., Illingworth, J.: 'Minimum error thresholding', *Pattern Recognit.*, 1986, **19**, (1), pp. 38–52
4 Padmanabhan, K., Eddy, W.F., Crowley, J.C.: 'A novel algorithm for optimal image thresholding of biological data', *J. Neurosci. Methods*, 2010, **193**, (2), pp. 380–384
5 Pun, T.: 'Entropy thresholding: a new approach', *Comput. Vision Graph. Image Process. Comput. Graphics Image Process.*, 1981, **16**, (3), pp. 210–239
6 Sathya, P.D., Kayalvizhi, R.: 'Optimal multilevel thresholding using bacterial foraging algorithm', *Expert Syst. Appl.*, 2011, **38**, (12), pp. 15549–15564
7 Wang, S., Chung, F., Xiong, F.: 'A novel image thresholding method based on parzen window estimate', *Pattern Recognit.*, 2008, **41**, (1), pp. 117–129
8 Otsu, N.: 'A threshold selection method from gray-level histograms', *IEEE Trans. Syst. Man Cybern.*, 1979, **9**, (1), pp. 62–66
9 Kapur, J.N., Sahoo, P.K., Wong, A.C.K.: 'A new method for gray-level picture thresholding using the entropy of the histogram', *Comput. Vis., Graph. Image Process.*, 1985, **29**, pp. 273–285
10 Sezgin, M., Sankur, B.: 'Survey over image thresholding techniques and quantitative performance evaluation', *J. Electron. Imaging*, 2004, **13**, (1), pp. 146–165
11 Oldham, K., Spanier, J.: 'The fractional calculus' (Academic Press, 1974)
12 Prodlubny, I.: 'Geometric and physical interpretation of fractional integration and fractional differentiation', *Fractional Calc. Appl. Anal.*, 2002, **5**, (4), pp. 367–386
13 Oustaloup, A., Linarès, H.: 'The CRONE path planning', *Math. Comput. Simul.*, 1996, **41**, pp. 209–217
14 Battaglia, J.L., Cois, O., Puigsegus, L., Oustaloup, A.: 'Solving an inverse heat conduction problem using a non-integer identified model', *Int. J. Heat Mass Transf.*, 2001, **44**, pp. 2671–2680

doi: 10.1049/iet-ipr.2010.0471

15 Ramus-Sermenta, C., Moreava, X., Novillanta, M., Oustaloupa, A., Levron, F.: 'Generalised approach on fractional response of fractal networks', *Chaos Solitons Fractals*, 2002, **14**, pp. 479–488
16 Mathieu, B., Melchior, P., Oustaloup, A., Ceyral, ch.: 'Fractional differentiation for edge detection', *Signal Process.*, 2003, **83**, pp. 2421–2432
17 Nakib, A., Oulhadj, H., Siarry, P.: 'A thresholding method based on two-dimensional fractional differentiation', *Image Vision Comput.*, 2009b, **27**, (9), pp. 1343–1357
18 Nakib, A., Oulhadj, H., Siarry, P.: 'Fractional differentiation and non-Pareto multiobjecitve optimization for image thresholding', *Eng. Appl. Artif. Intell.*, 2009a, **22**, (2), pp. 236–249
19 Ferdi, Y., Herbeuval, J.P., Charel, A.: 'Un filtre numérique basé sur la dérivation non-entière pour l'analyse du signal électrocardiographique', *Journal de l'Innovation et Technologie en Biologie et Médecine*, 2000, **21**, pp. 205–209
20 Grünwold, A.K.: 'Uber begrenzte derivationen und deren Anwendung Z. Angew', *Math. Phys.*, 1867, **12**, pp. 441–480
21 Leitnikov, A.V.: 'Theory of differentiation of fractional order', *Math. Sb.*, 1868, **3**, pp. 1–68
22 Chong, C., Raveendran, P., Mukundan, R.: 'Translation and scale invariants of Legendre moments', *Pattern Recognit.*, 2004, **37**, (1), pp. 119–129
23 Foulonneau, A., Charbonnier, P., Heitz, F.: 'Multi-reference shape priors for active contours', *Int. J. Comput. Vis.*, 2009, **81**, pp. 68–81
24 Hosny, K.M.: 'Exact legendre moment computation for gray level images', *Pattern Recognit.*, 2007, **40**, (12), pp. 3597–3605
25 Teague, M.R.: 'Image analysis via the general theory of moments', *J. Opt. Soc. Am.*, 1979, **70**, (8), pp. 920–930
26 Ng, H.: 'Automatic thresholding for defect detection', *Pattern Recognit. Lett.*, 2006, **27**, pp. 1644–1649
27 Sahoo, K.P., Arora, G.: 'Image thresholding using two dimensional Tsallis-Havrda-Charvat entropy', *Pattern Recognit. Lett.*, 2006, **27**, pp. 520–528
28 Berkeley University The Berkeley Segmentation Dataset and Benchmark, Grouping and Ecological Statistics, 2007, 2005. http://www.eecs.berkeley.edu/Research/Projects/CS/vision/grouping/